

The Shapes of Dense Cores and Bok Globules

Barbara S. Ryden ¹

Department of Astronomy, The Ohio State University,
174 W. 18th Ave., Columbus, OH 43210

ABSTRACT

The shapes of isolated Bok globules and embedded dense cores of molecular clouds are analyzed using a nonparametric kernel method, using the alternate hypotheses that they are randomly oriented prolate objects or that they are randomly oriented oblate objects. In all cases, the prolate hypothesis gives a better fit to the data. If Bok globules are oblate spheroids, they must be very flattened; the average axis ratio is $\langle \gamma \rangle \approx 0.3$, and no globules can have $\gamma \gtrsim 0.7$. If Bok globules are prolate, their intrinsic flattening is not as great, with a mean axis ratio $\langle \gamma \rangle \approx 0.5$. For most data samples of dense cores embedded within molecular clouds, the randomly-oriented oblate hypothesis can be rejected at the 99% one-sided confidence level. If the dense cores are prolate, their mean axis ratio is in the range $\langle \gamma \rangle = 0.4 \rightarrow 0.5$. Analysis of the data of Nozawa et al. (1991) reveals that dense cores are significantly different in shape from the clouds in which they are embedded. The shapes of dense cores are consistent with their being moderately flattened prolate spheroids; clouds have flatter apparent shapes, and are statistically inconsistent with a population of axisymmetric objects viewed at random angles.

Subject headings: ISM: clouds – ISM: globules – ISM: structure

1. Introduction

The molecular gas in our galaxy shows structure on a wide range of scales. The largest structures detected in the molecular gas are giant molecular clouds (GMCs), of which the largest have diameters of ~ 100 pc and masses of more than $10^6 M_{\odot}$. High resolution studies of molecular clouds, however, reveal that they have internal structure on all scales, and are typically clumpy or filamentary. Direct imaging of CO in nearby clouds reveals structure on all scales down to lengths of ~ 0.01 pc and masses of $\sim 0.01 M_{\odot}$ (Falgarone, Puget, & Pérault 1992; Langer et al. 1995). Studies of the time variability of absorption lines indicates the presence of structure in the dense

¹National Science Foundation Young Investigator; ryden@mps.ohio-state.edu

gas on scales down to lengths of $\sim 5 \times 10^{-5}$ pc and masses of $\sim 5 \times 10^{-9} M_{\odot}$ (Marscher, Moore & Bania 1993; Moore & Marscher 1995).

In this hierarchy of sizes, however, not all scales are of equal interest to astronomers. Stars form by gravitational collapse of dense regions within molecular clouds; much interest is therefore focused on the scale corresponding to the mass of protostars. Surveys of nearby clouds (within 500 parsecs of the earth) have focused attention on dense cores with typical diameters of ~ 0.1 pc, masses of $\sim 30 M_{\odot}$, and densities of $\sim 2 \times 10^4 \text{ cm}^{-3}$ (Myers, Linke, & Benson 1983; Benson & Myers 1989). In addition to dense cores embedded within GMCs, our galaxy also contains isolated dense clouds known as Bok globules (Bok & Reilly 1947). Neither dense cores nor Bok globules are spherical, as a general rule. The projected axis ratio, $q \equiv b/a$, of small Bok globules has an average value $\langle q \rangle \approx 0.6$ (Clemens & Barvainis 1988, hereafter CB; Bourke, Hyland, & Robinson 1995; hereafter BHR). Embedded dense cores are similarly flattened, with $\langle q \rangle \approx 0.5 - 0.6$ (Myers et al. 1991; Tatematsu et al. 1993).

The projected axis ratios of globules and cores are of interest because they place constraints on the intrinsic shapes of these objects. The intrinsic shapes of isolated globules and embedded cores are determined by a variety of physical processes. Globules and cores are sculpted by the self-gravity of the gas which they contain and by thermal pressure, turbulent pressure, and magnetic pressure. Since star formation occurs in these dense regions, their physical properties are further modified by outflows and winds from the protostars which may be embedded within them. Recent optical surveys of Bok globules (CB; BHR; Hartley et al. 1986) and millimeter surveys of dense cores (Benson & Myers 1989; Loren 1989; Lada, Bally, & Stark 1991; Nozawa et al. 1991) provide data sets of apparent axis ratios. As a cautionary note, however, it should be pointed out that a core or globule is not a solid, well-defined object with easily measurable axis ratios. It is merely one scale in a hierarchy of structure. The shape of a dense core as defined by the emission of one molecular line, moreover, will not be precisely the same as its shape defined by the emission of a different molecule. Readers are advised to regard the shapes measured in surveys with a certain amount of skepticism.

Previous studies (David & Verschueren 1987; Myers et al. 1991; Fleck 1992) have placed constraints on the permitted intrinsic shapes of dense cores. For instance, the mean apparent axis ratio $\langle q \rangle \approx 0.5 - 0.6$ for cores is fully consistent with a population of prolate objects, but only marginally consistent with an oblate population (Myers et al. 1991; Fleck 1992). More sophisticated analytic tools for examining sets of axis ratios have now been developed by investigators studying the intrinsic axis ratios of elliptical galaxies and other stellar systems. For instance, starting with a nonparametric estimate for the distribution $f(q)$ of apparent axis ratios, it is possible to find an estimate for the distribution $N(\gamma)$ of intrinsic axis ratios, given the assumption that the systems considered are either oblate or prolate spheroids and are randomly oriented with respect to the observer (Tremblay & Merritt 1995; Ryden 1996).

Using this technique, one is able, for instance, to test the hypothesis that all dense cores

or Bok globules are randomly oriented prolate objects. A test of the randomly oriented prolate hypothesis, more stringent than simply looking at the mean $\langle q \rangle$, is provided by examining the entire distribution $f(q)$. I first compute an estimate $\hat{f}(q)$ for the distribution of apparent axis ratios, then mathematically invert it to find a estimated distribution $\hat{N}_P(\gamma)$ of intrinsic axis ratios. The inversion is mathematically unique, but the resulting function \hat{N}_P is only physically meaningful if it is non-negative for all values of γ . If \hat{N}_P dips below zero at a statistically significant level, the initial hypothesis – that the cores or globules are randomly oriented prolate objects – can be rejected.

Similarly, one can test the hypothesis that cores or globules are randomly oriented oblate objects. The available kinematic information, however, indicates that dense cores are not rotationally supported oblate spheroids (Goodman et al. 1993). Large scale maps also show that many dense cores are aligned with larger filamentary structures, indicating that a prolate geometry is more likely in such cases (Myers et al. 1991). Thus, it should not be surprising when the randomly oriented oblate hypothesis turns out to be emphatically rejected for samples of dense cores.

In section 2, I give a brief outline of the mathematical techniques used to find the distribution of intrinsic axis ratios, given either the prolate or oblate hypothesis – a fuller description, for those who desire it, is given in Ryden (1996). In section 3, I apply these techniques to Bok globules, and in section 4, I apply them to dense cores embedded within molecular clouds. Generally speaking, for each data set considered, the prolate hypothesis gives a better fit than does the oblate hypothesis, given the assumption that the globules and cores are randomly oriented. In section 5, I discuss the implications of this finding for the origin and evolution of dense cores and globules.

2. Methods

I start with a sample q_1, q_2, \dots, q_N measured axis ratios for a sample of N globules or dense cores. The nonparametric kernel estimator for the underlying distribution $f(q)$ is

$$\hat{f}(q) = \frac{1}{Nh} \sum_{i=1}^N K\left(\frac{q - q_i}{h}\right), \quad (1)$$

where K is the kernel function. A discussion of kernel nonparametric estimators, as applied to astronomical problems, is given by Merritt & Tremblay (1994), Vio et al. (1994), and Merritt & Tremblay (1995). For my purposes, I want a smooth differentiable kernel, so I use a Gaussian:

$$K(x) = \frac{1}{\sqrt{2\pi}} e^{-x^2/2}. \quad (2)$$

For a kernel width h , I adopt

$$h = 0.9AN^{-0.2} , \quad (3)$$

where A is the smaller of the standard deviation of the sample and its interquartile range divided by 1.34 (Silverman 1986; Vio et al. 1994). For samples which are not strongly skewed, this formula for h is a good approximation to the value which minimizes the integrated mean square error in \hat{f} . For the samples examined in this paper, $0.06 < h < 0.10$.

Since $f(q)$ must be equal to zero for $q < 0$ and $q > 1$, reflective boundary conditions are applied at the boundaries $q = 0$ and $q = 1$ (Ryden 1996). The use of reflective boundary conditions ensures the proper normalization

$$\int_0^1 \hat{f}(q) dq = 1 . \quad (4)$$

One drawback of reflective boundary conditions is that they compel the slope of \hat{f} to be equal to zero at the boundaries, which might not be true of the actual distribution f . The shape of \hat{f} within a distance h of the boundaries should therefore be viewed with skepticism.

If the globules or cores in the sample are all randomly oriented oblate spheroids, then the estimated distribution $\hat{N}_O(\gamma)$ for the intrinsic axis ratio γ is given by the relation

$$\hat{N}_O(\gamma) = \frac{2\gamma\sqrt{1-\gamma^2}}{\pi} \int_0^\gamma \frac{d}{dq} (\hat{f}/q) \frac{dq}{\sqrt{\gamma^2 - q^2}} . \quad (5)$$

If the globules or cores are assumed to be randomly oriented prolate spheroids, then the estimated distribution $\hat{N}_P(\gamma)$ for the intrinsic axis ratio is

$$\hat{N}_P(\gamma) = \frac{2\sqrt{1-\gamma^2}}{\pi\gamma} \int_0^\gamma \frac{d}{dq} (q^2 \hat{f}) \frac{dq}{\sqrt{\gamma^2 - q^2}} . \quad (6)$$

If \hat{N}_O is negative for any value of γ , at a statistically significant level, then I can reject the hypothesis that the sample is drawn from a population of randomly oriented oblate objects. Either they are not all oblate, or they are not randomly oriented. Having a negative number of objects with a given value of γ is permissible from a purely mathematical viewpoint, but is nonsensical from a physical viewpoint. Similarly, if \hat{N}_P drops below zero at a statistically significant level, the randomly oriented prolate hypothesis can be rejected. The statistical significance of excursions below zero is estimated by bootstrap resampling techniques (Scott 1992; Merritt & Tremblay 1994). From the original data set q_1, q_2, \dots, q_N , I draw, with replacement, a new set of N data points. Using this bootstrap resampling of the original data, I compute new estimates for \hat{f} , \hat{N}_O , and \hat{N}_P . After making a large number n of these bootstrap estimates (for this paper, I used $n = 800$), confidence intervals can be placed on the original estimates \hat{f} , \hat{N}_O , and \hat{N}_P . At each value of γ , for instance, an upper limit can be placed on \hat{N}_O at the 99% one-sided confidence level, by finding the value of \hat{N}_O such that 1% of the bootstrap estimates lie above this value. If this upper confidence limit drops below zero, then the hypothesis that the objects are randomly oriented oblate spheroids can be rejected at the 99% confidence level. Similar analysis of \hat{N}_P

can be used to test the hypothesis that the objects in the original sample are randomly oriented prolate spheroids.

The confidence intervals derived from bootstrap resampling represent only the error resulting from finite sample size. Additional errors in the estimates \hat{f} , \hat{N}_O , and \hat{N}_P will be present as a result of errors in the measured values of q . If a typical measurement error σ_q is smaller than the smoothing length h , then the effects of measurement error can be ignored. The errors in the axis ratios of dense cores observed at millimeter wavelengths are relatively small, if the effects of the beamwidth are correctly subtracted (see section 4 below). However, the errors in the published axis ratios for surveys of Bok globules (CB; BHR) are significantly larger than h . A further complication is added by the fact that errors in q are generally not Gaussian, so they cannot simply be added in quadrature to the kernel width h . The presence of non-Gaussian errors in the measurement of the axis ratio of nearly circular objects can significantly affect the shape of \hat{f} when $q \sim 1$. This distortion of \hat{f} , in turn, can affect the conclusions which are drawn about the intrinsic shapes of the observed objects. A cautionary tale is related by Franx & de Zeeuw (1992), who deduced the intrinsic ellipticity ϵ of disk galaxies from their observed axis ratios. Assuming Gaussian errors in q , their best model had $\epsilon = 0.06$; however, the introduction of non-Gaussian errors led to a best fitting model with $\epsilon = 0$. In the following section, it will also be seen that the introduction of non-Gaussian rounding errors distorts the distribution $\hat{f}(q)$ for Bok globules.

3. Isolated Bok Globules

Bok globules are not, in general, spherical. Bok & Reilly (1947) defined globules as “approximately circular or oval dark objects of small size”, as contrasted to the “wind-blown wisps of dark nebulosity” which can also be found in the interstellar medium of our galaxy. CB constructed a catalog of small Bok globules with declination $\delta > -36^\circ$. They searched Palomar Observatory Sky Survey (POSS) plates for isolated, opaque globules with diameters less than $10'$. The axis ratio of the globules was explicitly not a selection criterion. Their complete catalog contains 248 objects, with a mean angular size of $4'$. The apparent axis ratio of each globule was determined by approximating its shape as an ellipse, and then measuring the minor and major axes of the fitted ellipse. The axis ratios measured for the complete sample ranged from $q = 1.00$ to $q = 0.14$, with a mean $\langle q \rangle = 0.59$ and standard deviation $\sigma_q = 0.23$.

To begin the analysis, I naïvely take the values for the axis length a and b published by CB, and use the resulting values of $q = b/a$ to find the estimated distribution $\hat{f}(q)$. The function \hat{f} determined in this way is shown as the solid line in the upper panel of Figure 1. In this Figure (and in every subsequent Figure in this paper), the dashed lines indicate the 80% confidence band and the dotted lines show the 98% confidence band, as determined by bootstrap resampling. The estimated distribution \hat{N}_O of intrinsic axis ratios, given the randomly oriented oblate hypothesis,

is shown in the middle panel of Figure 1. The estimated distribution \hat{N}_P of axis ratios, given the randomly oriented prolate hypothesis, is shown in the bottom panel. The most striking aspect of the estimate $\hat{f}(q)$ found in this manner is that it is bimodal. In addition to a broad maximum around $q \sim 0.55$, there is a second peak at $q = 1$. Does this bimodality indicate that there are two populations of globules, one flattened and one nearly spherical? No. The peak at $q = 1$ is an artifact, the result of rounding errors in q . CB, in measuring the axis lengths of globules on the POSS plates, rounded a and b to the nearest millimeter, corresponding to $1/12$ in angular scale. Many of the globules in the survey are quite small; 42 out of 248 have $a \leq 2$ mm. Consequently, rounding of the axis lengths can have a large effect on the measured value of q . For instance, a globule whose true size on the POSS plate is $1.6 \text{ mm} \times 2.4 \text{ mm}$ will be tabulated as being $2.0 \text{ mm} \times 2.0 \text{ mm}$. Its axis ratio will be erroneously computed as $q = 1.00$ instead of its true value of $q = 0.67$. A major effect of rounding errors is that small flattened globules will be incorrectly classified as being circular.

The effect of the non-Gaussian rounding errors can be approximately compensated for. To the values of a and b tabulated by CB for each globule, I add an error term Δ drawn uniformly from the interval $-0.56 < \Delta < 0.56$. I then compute the new values of q after the error terms are added on, and compute $\hat{f}(q)$. After repeating this process 800 times, with a different seed for the random number generator each time, I take the average value of the 800 estimates $\hat{f}(q)$ as the new best estimate of the underlying distribution $f(q)$, taking into account the errors introduced by rounding the axis lengths a and b . The best estimate found in this way is given as the solid line in the top panel of Figure 2. The 80% confidence bands (dashed lines) and the 98% confidence bands (dotted lines) include both the errors due to finite sample size and the errors in q due to rounding.

Note that when the rounding errors are compensated for, the peak at $q = 1$ disappears. The distribution \hat{f} now has a single maximum at $q = 0.6$. The mean value of q is $\langle q \rangle = 0.57$ and the standard deviation is $\sigma_q = 0.22$. The derived values of \hat{N}_O , given the oblate hypothesis, and \hat{N}_P , given the prolate hypothesis, are shown in the middle panel and bottom panel of Figure 2. The oblate hypothesis cannot quite be rejected at the 99% one-sided confidence level, but can be rejected at lower confidence levels. If the globules are all oblate spheroids, then they must be quite flattened. Few or no globules, if they are oblate, can have $\gamma \gtrsim 0.7$, and the peak in \hat{N}_O is at $\gamma \approx 0.25$. The observed axis ratios, when corrected for rounding errors, are fully consistent with the hypothesis that globules are all prolate objects with random orientations. The distribution \hat{N}_P (bottom panel of Figure 2) is everywhere positive, yielding a mean axis ratio $\langle \gamma \rangle = 0.48$ and standard deviation $\sigma_\gamma = 0.20$. The prolate hypothesis yields a broader range of intrinsic axis ratios than does the oblate hypothesis, with prolate globules ranging in shape from filamentary structures with $\gamma \sim 0.1$ to nearly spherical globules with $\gamma \sim 1$.

The catalog of CB in the northern sky is complemented by that of BHR in the southern sky. Starting with the comprehensive catalog of Hartley et al. (1986), which lists dark clouds with $\Delta < -33^\circ$, BHR selected highly opaque clouds with $a < 10'$. A total of 169 globules met their selection criteria. The axis lengths of the selected globules were measured from SERC Schmidt

survey plates. Axis lengths longer than $3'$ were rounded to the nearest arcminute; axis lengths shorter than $3'$ were rounded to the nearest 0.5 arcminute. This rounding of axis lengths was sufficient to create significant errors in the axis ratio q . Consequently, I computed the estimated distribution function $\hat{f}(q)$ using the correction technique described above. To axis lengths less than $3'$, I added an error Δ drawn uniformly from the interval $-0'.25 < \Delta < 0'.25$. For axis lengths greater than $3'$, $-0'.5 < \Delta < 0'.5$. The value of \hat{f} , including corrections for rounding errors, is given in the upper panel of Figure 3. The 80% and 98% confidence bands include the effects both of finite sample size and of rounding errors.

The BHR globules are slightly rounder on average than the CB globules; $\langle q \rangle = 0.61$ as compared to $\langle q \rangle = 0.57$. The standard deviation for each sample is $\sigma_q = 0.22$. In addition, the \hat{f} for the BHR globules lacks the dip at $q \approx 1$ which is seen in \hat{f} for the CB sample. The difference in apparent shapes for the CB sample and the BHR sample is a result of the difference in their definitions of a Bok globule, and not a reflection of differences in the properties of Bok globules in the northern and southern hemispheres.

The oblate distribution \hat{N}_O for the BHR sample is shown in the middle panel of Figure 3; it is consistent with the hypothesis that the globules are randomly oriented oblate spheroids. If so, however, they must be intrinsically quite flat, with a mean and standard deviation of $\langle \gamma \rangle = 0.33$ and $\sigma_\gamma = 0.15$; few or no globules can have $\gamma \gtrsim 0.7$. If, by contrast, the globules are randomly oriented prolate spheroids, they will have a broader range of intrinsic axis ratios, shown in the bottom panel of Figure 4. Under the prolate hypothesis, the mean and standard deviation of the intrinsic axis ratio are $\langle \gamma \rangle = 0.52$ and $\sigma_\gamma = 0.21$.

In conclusion, both the BHR and CB data sets show that the spherical approximation is a poor one for Bok globules; they must be intrinsically quite flat. The hypothesis that Bok globules are randomly oriented oblate objects cannot be excluded. If the globules are oblate, however, they must be quite flat, with a distribution peaking at $\gamma \sim 0.3$, and equal to zero at $\gamma \gtrsim 0.7$. If the Bok globules are randomly oriented prolate objects, they have a wider range of intrinsic axis ratios. Still, there are few nearly spherical globules, even under the prolate hypothesis. For the BHR sample, 21% of prolate globules have $\gamma \geq 0.7$; for the CB sample, only 14% of the prolate globules have $\gamma \geq 0.7$.

4. Embedded Dense Cores

Bok globules, according to Bok's original definition, are relatively well-defined and isolated objects. The CB and BHR catalogs of Bok globules contain only small globules. Their upper size limit of $10'$ corresponds to a linear scale of 0.7 pc at a distance of 500 pc. Small Bok globules are of interest to astronomers because their relative simplicity makes them good laboratories for testing theories of star formation. Most star formation in our galaxy, however, occurs not within simple

Bok globules but within the more complex environment of large molecular clouds. The dense cores of molecular clouds (with “dense” meaning $n \gtrsim 10^4 \text{ cm}^{-3}$) can be traced using the emission lines of CS (Lada et al. 1991) or NH_3 (Benson & Myers 1989). Each emission line probes a different density and temperature. Cores defined by CS emission have a larger velocity dispersion, density, and mass than the cores defined by NH_3 emission (Zhou et al. 1989). However, Myers et al. (1991), by mapping dense cores in the lines of NH_3 , CS, and C^{18}O , have demonstrated that the maps in the different lines are similar (but not identical) in position, orientation, and elongation. Thus, it seems that the observed shapes of cores are not strongly dependent on the particular emission line which is chosen for the purpose of observation.

Benson & Myers (1989) made a search for dense cores in the $(J, K) = (1, 1)$ rotation inversion line of NH_3 . They surveyed 149 positions selected to be in the center of opaque regions on POSS plates. The dark clouds selected in this manner are mainly nearby, with 119 of the 149 clouds known to be less than 500 pc away. Of the 149 regions surveyed, 66 were detected in NH_3 . Of the regions where NH_3 was detected, 37 were mapped, and had their apparent axis ratios measured. Of the mapped regions, 26 were identified as being dense cores embedded within a larger molecular complex (type C), 5 were identified as being isolated globules (type G), and 6 were classified as type M, intermediate between types C and G. A Kolmogorov-Smirnov (KS) test comparing the 26 type C cores to the 11 type M and G cores reveals no significant difference in their distribution of apparent axis ratios ($P_{\text{KS}} = 0.86$). For the purposes of my analysis, therefore, I will lump all the mapped regions together, and refer to them as “dense cores”. In addition to the dense cores selected from POSS plates, Benson & Myers provided maps and axis ratios for an additional 4 dense cores, selected for observation because they were in the same position as an IRAS point source. Estimated masses of the 41 mapped dense cores lie in the range $0.5 M_{\odot} < M < 760 M_{\odot}$, with a median of $13 M_{\odot}$.

The upper panel of Figure 4 shows the estimated distribution $\hat{f}(q)$ for the distribution of apparent axis ratios for all 41 dense cores mapped by Benson & Myers (1989). The mean apparent flattening ($\langle q \rangle = 0.59$) for this sample is comparable to the mean for the BHR and CB samples of Bok globules. However, the Benson & Myers dense cores are notably lacking in nearly circular objects; the maximum axis ratio in the entire sample is $q = 0.89$. The lack of nearly circular objects is the classic indication that a population cannot consist of randomly oriented oblate spheroids. Indeed, the oblate hypothesis can be rejected at a very high confidence level – the middle panel of Figure 4 shows that \hat{N}_O dips far below zero for $\gamma \gtrsim 0.8$. So great is the paucity of nearly circular cores that even the randomly oriented prolate hypothesis can be rejected at the 99% confidence level (see the bottom panel of Figure 4). In short, the Benson & Myers sample of dense cores cannot be a population of randomly oriented axisymmetric objects. Either they contain a significant number of triaxial cores or there is a selection effect which excludes axisymmetric cores from the sample when their axis of symmetry is close to the line of sight. Compared to populations of axisymmetric objects, populations of triaxial objects provide a better fit to samples with a lack of apparently circular objects. This is because triaxial objects appear to be nearly circular from

only a very limited range of viewing angles (Binggeli 1980; Binney & de Vaucouleurs 1981).

Of the dense cores mapped by Benson & Myers (1989), 21 have IRAS point sources within one core diameter of the core’s center. The IRAS point sources are most plausibly explained as being protostars or young stars embedded within the dense core. It is not absurd to speculate that dense cores with embedded IRAS sources could have different shapes, on average, than cores without IRAS sources. For instance, cores of a particular shape might be more efficient at collapsing to form stars. In addition, an embedded protostar, in pouring out matter and radiation, might change the shape of the core which encloses it. However, it turns out that there is no significant difference between the distribution of q for the 21 cores with embedded IRAS sources and the distribution for the 20 cores without IRAS sources. A KS test comparing the two distributions yields $P_{\text{KS}} = 0.9987$, indicating a remarkably close similarity between the two distributions. The similarity in axis ratios occurs in spite of the fact that the cores with embedded sources have significantly larger radii, masses, and line widths than the cores without sources (Benson & Myers 1989). Perhaps there is a preferred range of shapes for NH_3 cores, which does not depend on the size of the core or whether it contains an embedded protostar.

The dense cores mapped by Benson & Myers exist lie within many separate molecular clouds, with a wide range in galactic longitude. To eliminate the variance which may exist between the cores of different molecular clouds, with different physical and chemical properties, it is useful to look at the population of dense cores embedded within a single molecular cloud. Lada et al. (1991) studied the dense cores of Lynds 1630 (alias Orion B), a molecular cloud containing $\sim 10^5 M_{\odot}$ of gas (Maddalena et al. 1986), located ~ 400 pc away (Hilton & Lahulla 1995). Lada et al. mapped the cloud using the $J = 2 \rightarrow 1$ transition of CS, using a beamwidth of $1'.8$ (corresponding to 0.21 pc).

Lada et al. (1991) identified individual “clumps” within Lynds 1630. A clump was identified as a closed volume in position-velocity space, containing CS emission at a 5σ level above the noise. The entire region surveyed contained 42 clumps, as defined in this manner. Shapes of individual clumps were determined by measuring the major and minor axis lengths of the 5σ contours on the sky, subtracting the beamwidth in quadrature. The majority of the clumps were unresolved, but measured axis ratios were provided for 19 clumps with corrected major axis length greater than the beamwidth ($2a > 1'.8$). Virial masses for these clumps lie in the range $8 M_{\odot} < M < 460 M_{\odot}$, with a median of $104 M_{\odot}$. Although 19 is not a large number, and consequently the derived error bands on \hat{f} and \hat{N} are large, it is still interesting to compare the shapes of the Lynds 1630 clumps to the more eclectic dense cores of Benson & Myers (1989). The 19 cores of Lada et al. (with a mean and standard deviation in q of 0.55 ± 0.19) have a distribution of apparent shapes similar to that of the 41 dense cores of Benson & Myers (with a mean and standard deviation of 0.59 ± 0.19). A KS test comparing the two distributions yields $P_{\text{KS}} = 0.70$. The nonparametric estimate $\hat{f}(q)$ for the Lada et al. clumps is shown in the upper panel of Figure 5. Because of the small number of clumps, the oblate hypothesis cannot be excluded at the 99% one-sided confidence level (see the middle panel of Figure 5). However, if the clumps are oblate and randomly oriented, then

they must all be quite flat, just as in the case of the Bok globules studied by BHR and CB. The best-fitting function \hat{N}_O peaks at $\gamma \sim 0.4$, and there can be few or no oblate clumps with $\gamma \gtrsim 0.6$. Conversely, the randomly oriented prolate hypothesis, as illustrated in the bottom panel of Figure 5, is statistically more acceptable, and yields a broader range of intrinsic axis ratios. The best-fitting function \hat{N}_P yields a mean axis ratio $\langle \gamma \rangle = 0.46$ and a standard deviation $\sigma_\gamma = 0.17$.

Another molecular cloud which has been surveyed for dense cores is the ρ Ophiuchus cloud. Its center is located at approximately $b = 17^\circ$, $l = 355^\circ$ and is at a distance of 160 pc from the sun. Its total mass is estimated to be $\sim 3000 M_\odot$ (Loren 1989). Thus, although smaller than Orion B, the ρ Oph cloud is closer, and can be mapped at higher resolution. Loren (1989) mapped the ρ Oph cloud using the $J = 1 \rightarrow 0$ transition of ^{13}CO . The telescope beamwidth was 2.4 FWHM, corresponding to a spatial resolution of 0.11 pc. The catalog of Loren (1989) contains 89 “clumps”, located at maxima of the emission in velocity-position space. Each clump must be clearly separated from other clumps in order to be included in the catalog. The masses estimated from the integrated ^{13}CO intensity lie in the range $0.6 M_\odot < M < 850 M_\odot$, with a median of $8.8 M_\odot$. The major and minor axis lengths of each clump are the FWHM along the principal axes, projected onto the sky (the beamwidth is subtracted in quadrature). The definition of a “clump” and of its major and minor axis lengths thus differ from the definitions used by Lada et al. (1991); be cautious in comparing the two different types of clump.

The estimated distribution $\hat{f}(q)$ for the Loren clumps (upper panel of Figure 6) is marked by a scarcity of objects with $q \gtrsim 0.8$. Of 89 clumps, only 6 have $q > 0.8$. The distribution of q for the clumps of Loren (1989) is significantly different at the 98% confidence from that for the dense cores of Benson & Myers (1989); a K-S test yields $P_{\text{KS}} = 0.015$. The Loren clumps are flatter, on average, than the Benson & Myers cores, with a mean and standard deviation in q of 0.48 ± 0.20 . The difference between the clump shapes found by Loren (1989) and those found by Lada et al. (1991) is not statistically significant: $P_{\text{KS}} = 0.41$. Because of the lack of nearly circular clumps in the Loren sample, the randomly oriented oblate hypothesis can be rejected at the 99% confidence level; see the middle panel of Figure 6. The prolate hypothesis, however, is statistically acceptable, as shown in the bottom panel of Figure 6. If the clumps are randomly oriented prolate objects, they must be quite flat, with $\langle \gamma \rangle = 0.39$ and $\sigma_\gamma = 0.17$, and with very few clumps having $\gamma > 0.7$.

The dense cores and clumps observed by the various surveys differ somewhat in their definitions. Their masses, however, all lie in the range $0.5 M_\odot < M < 900 M_\odot$, and their characteristic density is $\sim 10^4 \text{ cm}^{-3}$. Broadly speaking, the dense cores and clumps are more readily explained by the prolate hypothesis than by the oblate hypothesis. This conclusion results from the lack of nearly circular objects in the samples. The cores and clumps must be intrinsically quite nonspherical; if they are randomly oriented prolate objects, the mean axis ratio is approximately $\gamma \sim 0.4$.

In focusing solely on the dense cores of molecular clouds, however, I have been neglecting the larger structures within clouds. Molecular clouds show substructure on all resolvable scales,

including scales larger and smaller than individual dense cores. The existence of hierarchical structure on such a broad range of scales has prompted investigators to describe molecular clouds in terms of their fractal dimension (Dickman, Horvath, & Margulis 1990; Falgarone, Phillips, & Walker 1991). However, different physical processes dominate at different length scales, which makes it unlikely that the structure is a perfectly self-similar fractal. To investigate the dependence of the shape of substructure upon size, I can use the molecular survey of Nozawa et al. (1991), who identified and cataloged substructures of different size in their survey.

Nozawa et al. (1991) mapped an area in the Ophiuchus region using the $J = 1 \rightarrow 0$ transition of ^{13}CO . The telescope beamwidth was $2'.7$ FWHM. The area mapped ($b = 15^\circ \rightarrow 33^\circ$; $l = 355^\circ \rightarrow 12^\circ$) is north of the ρ Ophiuchus main cloud mapped by Loren (1989). Nozawa et al. picked out two types of substructure in their survey. The larger substructures, which they call “clouds”, are defined as the regions enclosed by the 3σ contours in the integrated ^{13}CO map. The map contains 23 clouds defined in this manner, with estimated masses in the range $13 M_\odot < M < 1200 M_\odot$. The median cloud mass was $76 M_\odot$. The smaller substructures, called “cores”, are defined as maxima in the integrated ^{13}CO emission. Thus, each cloud contains at least one core; the largest cloud contains 8 separate cores. The total number of cores mapped by Nozawa et al. (1991) is 51 (including 3 cores not well resolved at $2'.7$). The axis ratios of the cores were estimated by finding the contour at the half peak intensity level and fitting the contour with an ellipse. The estimated core masses lie in the range $3 M_\odot < M < 160 M_\odot$, with a median mass of $13 M_\odot$. The mass of each core is from 0.6% to 48% of the mass of the cloud in which it is embedded.

The “cores” in the ^{13}CO map of Nozawa et al. (1991) are slightly larger, on average, than the “clumps” in the ^{13}CO map of Loren (1989). The two populations, however, do not have different distributions of axis ratios at a high statistical confidence level. Comparison of the axis ratios of the two populations, using a KS test, yields $P_{\text{KS}} = 0.18$. The most noticeable difference between the two populations is that the cores of Nozawa et al. (1991) are rounder; they have a mean and standard deviation in q of 0.57 ± 0.21 , as compared to 0.48 ± 0.20 for the Loren (1989) clumps.

The best-fitting estimate $\hat{f}(q)$ for the cores of Nozawa et al. (1991) is shown in the upper panel of Figure 7. Once again, we see a dip in \hat{f} as $q \rightarrow 1$. However, the dip is not as deep or as wide as in the case of the Loren (1989) clumps, shown in Figure 6. As a result, the randomly oriented oblate hypothesis cannot be rejected at the 90% confidence level for the Nozawa cores (see the middle panel of Figure 7). If the oblate hypothesis is true, however, the cores must be very flat, with \hat{N}_O peaking at $\gamma \sim 0.3$, and with few or no cores having $\gamma \gtrsim 0.6$. The prolate hypothesis gives a better fit to the observations (see the bottom panel of Figure 7). If the Nozawa cores are randomly oriented prolate objects, then the mean axis ratio is $\langle \gamma \rangle = 0.48$, with a standard deviation of $\sigma_\gamma = 0.19$. The results for the *cores* of Nozawa et al. (1991) are thus similar to the results found for other dense cores and for Bok globules; the prolate hypothesis gives a better fit than the oblate hypothesis, and if the oblate hypothesis is insisted upon, then the cores must all be quite flat. But what can be deduced about the shapes of the *clouds*, which are larger than the

cores?

The clouds in the catalog of Nozawa et al. (1991) are distinctly different in shape from the smaller, denser cores which are embedded within them. A KS test comparing the 23 clouds with the 48 resolved cores yields $P_{\text{KS}} = 2 \times 10^{-3}$. The clouds are generally elongated filaments, with a mean and standard deviation in their axis ratio of $\langle q \rangle = 0.39$ and $\sigma_q = 0.17$. The most elongated cloud, with $q = 0.07$, is also the most massive, with an estimated mass $M = 1200 M_{\odot}$. The estimated $\hat{f}(q)$ for the clouds, shown in the upper panel of Figure 8, peaks at $q = 0.3$ and goes to zero at $q = 1$. The severe lack of nearly spherical clouds means that the hypothesis of randomly oriented oblate clouds can be strongly ruled out. The 99% upper confidence band of \hat{N}_O (seen in the middle panel of Figure 8) dips well below zero. The roundest object in the sample of clouds has $\gamma = 0.7$. The distribution of oblate objects which minimizes the number of apparently circular objects is a population of infinitesimally thin disks ($\gamma = 0$); this population, when placed at random orientations, produces a distribution $f(q)$ which is uniform between $q = 0$ and $q = 1$. The probability that a sample of 23 infinitesimally thin disks, seen at random angles, produces no projections with $q > 0.75$ is only $P = (0.75)^{23} \approx 1.3 \times 10^{-3}$. Any other population of oblate objects would produce an even smaller value of P . The lack of nearly circular objects in the sample of clouds can even be used to rule out the hypothesis that the clouds are randomly oriented prolate objects. In the bottom panel of Figure 8, showing \hat{N}_P , the one-sided 99% confidence level drops below zero for $\gamma > 0.84$. Thus, either the clouds are intrinsically triaxial, or there is a selection effect which eliminates prolate clouds whose axes of symmetry lie close to the line of sight.

5. Discussion

Bok globules and dense molecular cloud cores, with densities $n \gtrsim 10^4 \text{ cm}^{-3}$, are of particular interest to astronomers because they are where stars form; see Myers (1985) and Shu, Adams, & Lizano (1987) for reviews. The assumption of spherical symmetry in a star-forming dense core is seductive from a theoretical viewpoint. It allows analytic calculations of collapse, such as the self-similar isothermal solution of Shu 1977), and permits numerical simulations with very high resolution. However, the observations reveal that the spherical assumption is a poor one. In the samples analyzed in this paper, the mean apparent axis ratio ranges from $\langle q \rangle = 0.48$ for the clumps observed by Loren (1989) to $\langle q \rangle = 0.61$ for the Bok globules cataloged by BHR. The intrinsic axis ratios are even more elongated than the projected axis ratios. Under the prolate hypothesis, the mean intrinsic axis ratio is $\langle \gamma \rangle = 0.39$ for the Loren (1989) sample and $\langle \gamma \rangle = 0.53$ for the BHR sample.

For each of the samples analyzed, the prolate hypothesis (that all cores and globules are randomly oriented prolate spheroids) yields a better fit to the observed distribution of axis ratios than does the oblate hypothesis. This conclusion agrees with other indications that cores and

globules are primarily prolate objects. For instance, cores are unlikely to be rotating oblate spheroids. In a sample of dense cores ($n \gtrsim 10^4 \text{ cm}^{-3}$) studied by Goodman et al. (1993), only 29 of 43 had a statistically significant velocity gradient. The measured gradients lie in the range $0.3 \rightarrow 4 \text{ km s}^{-1} \text{ pc}^{-1}$, with a typical ratio of rotational energy to gravitational energy of only ~ 0.02 . In addition, no correlation was found between the rotation axis and the projected short axis of the core, indicating that the cores are not rotationally supported oblate objects. Moreover, a study of the few molecular clouds with large velocity gradients (Arquilla & Goldsmith 1986) shows that clouds with significant gradients often have velocity fields which are more complicated than would be produced by simple rotation. If cores are shaped not by rotation but by anisotropic gravitational fields (Fleck 1992), then the extremely elongated cores ($q \lesssim 0.3$) must be prolate rather than oblate. A study of the environment of dense cores offers hints that at least some cores must be prolate. Of the 16 cores studied by Myers et al. (1991), 6 are observed to have their long axes aligned with larger filamentary structures, which are almost certainly prolate because of their extreme axis ratios ($q \sim 0.1$).

The tendency for dense cores to be embedded in long filaments of lower density matter was noted by Schneider & Elmegreen (1979), who compiled a catalog of “globular filaments”, defined as long filamentary dark clouds with globule-like dense cores spaced evenly along the filament. The distance between the dense cores in a globular filament is equal to 3 times the diameter of the cores. The work of Nozawa et al. (1991) confirms the general picture of cores being prolate objects with $q \sim 0.6$ embedded within larger, lower density, more filamentary ($q \sim 0.4$) clouds. Although the long axes of the dense cores tend to be aligned with the larger filaments in which they are embedded (Myers et al. 1991), being embedded within a larger structure does not greatly affect their shape. Embedded cores have shapes similar to those of isolated globules. Direct comparison of optically selected Bok globules (BHR; CB) to dense cores detected at millimeter wavelengths (Benson & Myers 1989; Lada et al. 1991; Loren 1989; Nozawa et al. 1991) is something that should only be done with caution. However, the shapes of the embedded (type C) cores in the Benson & Myers (1989) sample are indistinguishable from the shapes of the isolated (type G) cores.

For all the samples of dense objects in this sample, whether they are called globules, cores, or clumps, the best-fitting estimate $\hat{f}(q)$ dips below one as $q \rightarrow 1$. As a consequence, $\hat{N}_O(\gamma)$ dips below zero, and the hypothesis that the objects are randomly oriented oblate spheroids can be rejected at some confidence level. For some samples – the dense cores of Benson & Myers (1989) and the clouds of Nozawa et al. (1991) – the best-fitting estimate \hat{N}_P drops below zero. For these populations, we can reject the hypothesis of randomly oriented prolate spheroids. Previously, I have concentrated on the implications if the assumption of oblateness or prolateness is incorrect, and the objects are actually triaxial. But what if the other assumption I’ve made is incorrect, and the objects in the sample are not randomly oriented? Neighboring cores on a long filament, for instance, will tend to have their long axes pointing in the same direction (Nozawa et al. 1991). This correlation in the orientation angle will reduce the effective number of independent viewing

angles. Thus, the assumption of independent random viewing angles is incorrect in this case, and the error bands placed on \hat{f} , \hat{N}_O , and \hat{N}_P by bootstrap resampling will be underestimates. Relaxing the assumption that the orientations of cores are uncorrelated thus makes it more difficult to rule out the hypotheses that the cores are all oblate or all prolate.

It is not always obvious which assumption is incorrect when a particular hypothesis is rejected. For instance, I rejected the hypothesis that the clouds in the Nozawa et al. (1991) sample are randomly oriented prolate spheroids. This rejection is based on the lack of nearly circular clouds in the sample. Perhaps the assumption of random orientations is incorrect, and prolate clouds whose axis of symmetry lies close to the line of sight have been excluded from the sample. An examination of the maps of the clouds (Nozawa et al. 1991) reveals, however, that the other assumption – that the clouds are intrinsically prolate, must be incorrect. In projection, the clouds with the greatest apparent elongation are not ellipses, but are arc-shaped. The major axis of the cloud, in some cases, has a radius of curvature comparable to the axis length. This curvature of filaments is also seen in the “globular filaments” of Schneider & Elmegreen (1979). The long, filamentary clouds must be intrinsically curved, which prevents them from appearing exactly circular in projection from any angle.

On scales larger than dense cores, and with mean densities lower than $n \sim 10^4 \text{ cm}^{-3}$, the distribution of molecular gas is generally described as filamentary, wispy, or cobwebby, with gas lying in long, curved filaments. Dense cores and Bok globules, however, have less extreme axis ratios. It is not known which forces are dominant in determining the shape of cores and globules. It is possible, though, to state some forces which are not greatly significant. Since the shape of cores and globules is independent of whether they are embedded in larger structures (Benson & Myers 1989), external forces such as gravitational tidal forces cannot determine the shapes in the majority of cases. The shapes of cores also is independent of whether they contain embedded protostars (Benson & Myers 1989), so outflows and radiation pressure from protostars cannot have a significant effect on the overall shape of the core or globule in which it is embedded. Since nearly all cores are slowly rotating (Goodman et al. 1993), rotational flattening does not play an important role. The dense cores are not collapsing on a freefall timescale. The dynamical time for a core with $n \sim 10^4 \text{ cm}^{-3}$ is $t_{\text{dyn}} \sim 10^6 \text{ yr}$; the low efficiency of star formation in cores and globules – $\varepsilon \sim 0.3\%$ in the northern Ophiuchus region, for instance (Nozawa et al. 1991) – means that clouds are contracting on timescales much longer than their dynamical time. Thus, the “pancaking” effect of anisotropic collapse (Lynden-Bell 1964; Lin, Mestel, & Shu 1965) is not what flattens cores and globules.

Dense cores and globules, it is generally proposed, are supported by a combination of thermal pressure, turbulent pressure, and magnetic pressure. For all but the smallest cores, the observed line widths are greater than would be produced by thermal broadening alone. Temperatures in dense cores and Bok globules are typically $\sim 10 \text{ K}$. For ^{13}CO , thermal velocities alone produce a FWHM of $\Delta V = 0.13 \text{ km s}^{-1} (T/10 \text{ K})^{1/2}$. The observed width of ^{13}CO absorption lines is $\Delta v = 0.73 \rightarrow 2.24 \text{ km s}^{-1}$ for the Lada et al. (1991) clumps and $\Delta v = 0.5 \rightarrow 1.8 \text{ km s}^{-1}$ for the

Nozawa et al. (1991) cores. Supersonic velocities are seen within Bok globules as well. When the BHR globules were observed in NH_3 emission (Bourke et al. 1995), the intrinsic linewidth in globules where ammonia was strongly detected was $\Delta v = 0.28 \rightarrow 1.02 \text{ km s}^{-1}$, where thermal broadening would produce $\Delta v = 0.16 \text{ km s}^{-1}$ at a temperature of 10 K. The additional broadening can be explained as the result of turbulent motions within the globule or core (Larson 1981). However, it seems that the shape of cores is not crucially dependent upon the extent to which it is supported by turbulence. Benson & Myers (1989) found that the mean linewidth for cores without embedded IRAS sources is $\Delta v = 0.27 \text{ km s}^{-1}$ is significantly narrower than the mean width for cores with embedded sources, $\Delta v = 0.45 \text{ km s}^{-1}$, despite the fact that their kinetic temperatures are all $\sim 10 \text{ K}$. Although the cores with sources contain a higher fraction of turbulent kinetic energy, their distribution of apparent shapes is indistinguishable from that of cores without sources.

Magnetic forces can also play a significant role in determining the structure of dense cores (McKee et al. 1993). Although measuring magnetic fields in molecular clouds is a tricky business, available measurements indicate that magnetic pressure and turbulent pressure are of comparable importance in supporting cores against collapse (Myers & Goodman 1988). The presence of magnetic flux is certainly capable of influencing the size and shape of gaseous clumps. As an example, consider the scenario in which dense cores form by gravitational condensation along a filament – a proposed method for the formation of globular filaments (Schneider & Elmegreen 1979; Elmegreen 1985). The filament will break into globules whose separation is equal to the wavelength λ_m of the most rapidly growing instability. In the absence of a magnetic field, $\lambda_m = 5.4D$, where D is the initial diameter of the filament (Chandrasekhar & Fermi 1953). If the filament is aligned with a magnetic flux, however, λ_m will be increased. In the real interstellar medium, where the geometry of the magnetic field and the gas distribution is far more complicated, the shape of dense cores and Bok globules is determined by nonlinear magnetohydrodynamic turbulence whose study will require sophisticated numerical simulations. It is possible that the observed shapes of Bok globules and dense cores will act as constraints on future studies. It is also possible that the characteristic distribution $f(q)$ which is observed, peaking at $q \sim 0.4 \rightarrow 0.6$ and falling below $f = 1$ as $q \rightarrow 1$, is a generic result for a wide range of initial conditions and evolutionary histories.

I thank R. Barvainis, D. Clemens, R. Fleck, R. Pogge, and K. Sellgren for their advice and assistance, and the onymous referee, N. Evans, for his exceptionally helpful report. This work was supported by NSF grant AST-9357396.

REFERENCES

- Arquilla, R., & Goldsmith, P. F. 1986, *ApJ*, 303, 356
 Benson, P. J., & Myers, P. C. 1989, *ApJS*, 71, 89

- Binggeli, B. 1980, *A&A*, 82, 289
- Binney, J., & de Vaucouleurs, G. 1981, *MNRAS*, 194, 679
- Bok, B., & Reilly, E. 1947, *ApJ*, 105, 255
- Bourke, T. L., Hyland, A. R., & Robinson, G. 1995, *MNRAS*, 276, 1052 (BHR)
- Bourke, T. L., Hyland, A. R., Robinson, G., James, S. D., & Wright, C. M. 1995, *MNRAS*, 276, 1067
- Chandrasekhar, S., & Fermi, E. 1953, *ApJ*, 118, 116
- Clemens, D. P., & Barvainis, R. 1988, *ApJS*, 68, 257 (CB)
- David, M., & Verschueren, W. 1987, *A&A*, 186, 295
- Dickman, R. L., Horvath, M. A., & Margulis, M. 1990, *ApJ*, 365, 586
- Elmegreen, B. G. 1985, in *Protostars & Planets II*, ed. D. C. Black & M. S. Matthews (Tucson: U. of Arizona Press), 33
- Falgarone, E., Phillips, T. G., & Walker, C. K. 1991, *ApJ*, 378, 186
- Falgarone, E., Puget, J.-L., & Pérault, M. 1992, *A&A*, 257, 715
- Fleck, R. C. 1992, *ApJ*, 401, 149
- Franx, M., & de Zeeuw, P. T. 1992, *ApJ*, 392, L47
- Goodman, A. A., Benson, P. J., Fuller, G. A., & Myers, P. C. 1993, *ApJ*, 406, 528
- Hartley, M., Manchester, R. N., Smith, R. M., Tritton, S. B., & Goss, W. M. 1986, *A&AS*, 63, 27
- Hilton, J., & Lahulla, J. F. 1995, *A&AS*, 113, 325
- Lada, E. A., Bally, J., & Stark, A. A. 1991, *ApJ*, 368, 432
- Langer, W. D., Velusamy, T., Kuiper, T. B. H., Levin, S., Olsen, E., & Migenes, V. 1995, *ApJ*, 453, 293
- Larson, R. B. 1981, *MNRAS*, 194, 809
- Lin, C. C., Mestel, L., & Shu, F. H. 1965, *ApJ*, 142, 1431
- Loren, R. B. 1989, *ApJ*, 338, 902
- Lynden-Bell, D. 1964, *ApJ*, 139, 1195
- Maddalena, R. J., Morris, M., Moscowitz, J., Thaddeus, P. 1986, *ApJ*, 303, 375
- Marscher, A. P., Moore, E. M., & Bania, T. M. 1993, *ApJ*, 419, L101
- McKee, C. F., Zweibel, E. G., Goodman, A. A., & Heiles, C. 1993, in *Protostars & Planets III*, ed. E. H. Levy & J. I. Lunine (Tucson: U. of Arizona Press), p. 327
- Merritt, D., & Tremblay, B. 1994, *AJ*, 108, 514
- Moore, E. M., & Marscher, A. P. 1995, *ApJ*, 452, 679

- Myers, P. C. 1985, in *Protostars & Planets II*, ed. D. C. Black & M. S. Matthews (Tucson: U. of Arizona Press), 81
- Myers, P. C., Fuller, G. A., Goodman, A. A., & Benson, P. J. 1991, *ApJ*, 376, 561
- Myers, P. C., & Goodman, A. A. 1988, *ApJ*, 329, 392
- Myers, P. C., Linke, R. A., & Benson, P. J. 1983, *ApJ*, 264, 517
- Nozawa, S., Mizuno, A., Teshima, Y., Ogawa, H., & Fukui, Y. 1991, *ApJS*, 77, 647
- Ryden, B. S. 1996, *ApJ*, 461, 146
- Schneider, S., & Elmegreen, B. G. 1979, *ApJS*, 41, 87
- Scott, D. W. 1992, *Multivariate Density Estimation* (New York: Wiley)
- Shu, F. H. 1977, *ApJ*, 214, 488
- Shu, F. H., Adams, F. C., & Lizano, S. 1987, *ARA&A*, 25, 23
- Silverman, B. W. 1986, *Density Estimation for Statistics and Data Analysis* (New York: Chapman & Hall)
- Tatematsu, K., et al. 1993, *ApJ*, 404, 643
- Tremblay, B., & Merritt, D. 1995, *AJ*, 110, 1039
- Vio, R., Fasano, G., Lazzarin, M., & Lessi, O. 1994, *A&A*, 289, 640
- Zhou, S., Wu, Y., Evans, N. J., Fuller, G. A., & Myers, P. C. 1989, *ApJ*, 346, 168

Fig. 1.— *Top*, nonparametric kernel estimate of the distribution of apparent axis ratios for a sample of 248 northern Bok globules (Clemens & Barvainis 1988). The axis ratios are *not* corrected for rounding errors. *Middle*, distribution of intrinsic axis ratios, assuming that the globules are oblate. *Bottom*, distribution of intrinsic axis ratios, assuming that the globules are prolate. The solid line in each panel is the best estimate, the dashed lines are the 80% confidence band, found by bootstrap resampling, and the dotted lines are the 98% confidence band. The kernel width is $h = 0.067$.

Fig. 2.— As Fig. 1, but the apparent axis ratios of Clemens & Barvainis (1988) are corrected for rounding errors in the published catalog, using the method described in the text. The kernel width is $h = 0.063$.

Fig. 3.— As Fig. 1, but for a sample of 169 southern Bok globules (Bourke, Hyland, & Robinson 1995). The axis ratios are corrected for rounding errors. The kernel width is $h = 0.069$.

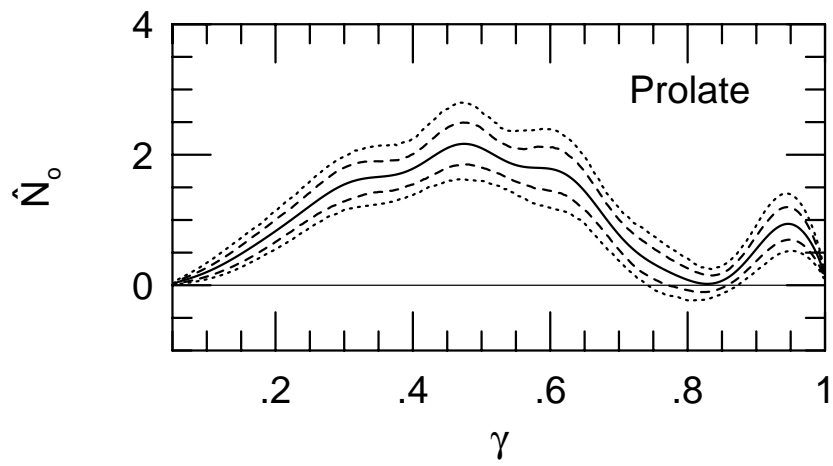
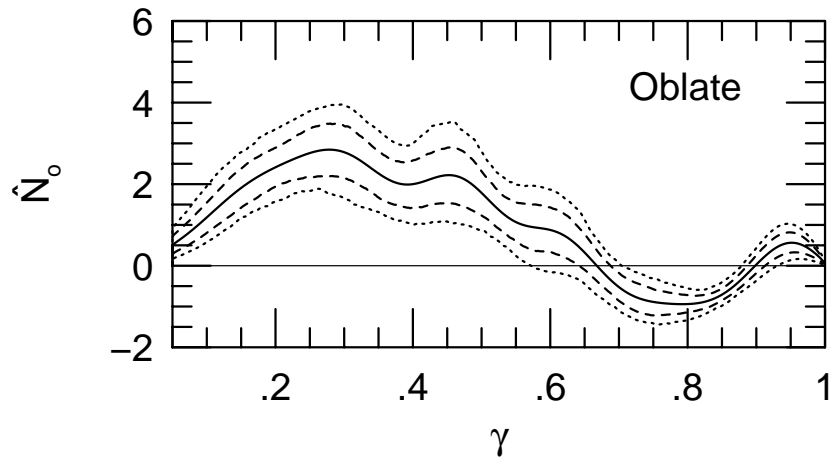
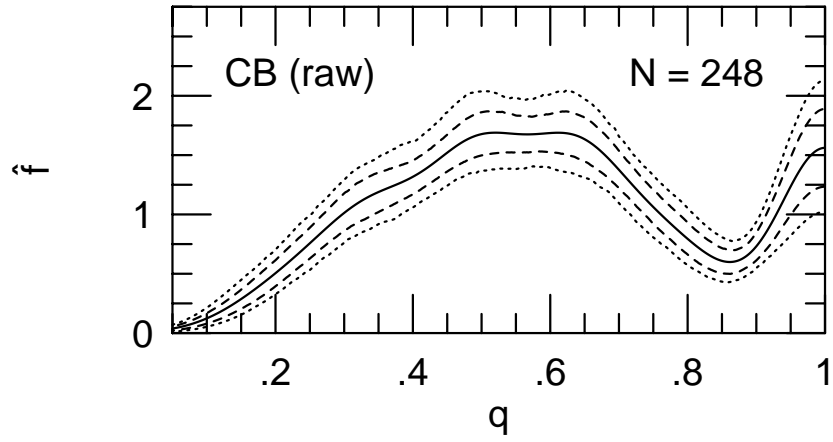
Fig. 4.— As Fig. 1, but for a sample of 41 dense cores in nearby molecular clouds (Benson & Myers 1989). The kernel width is $h = 0.080$.

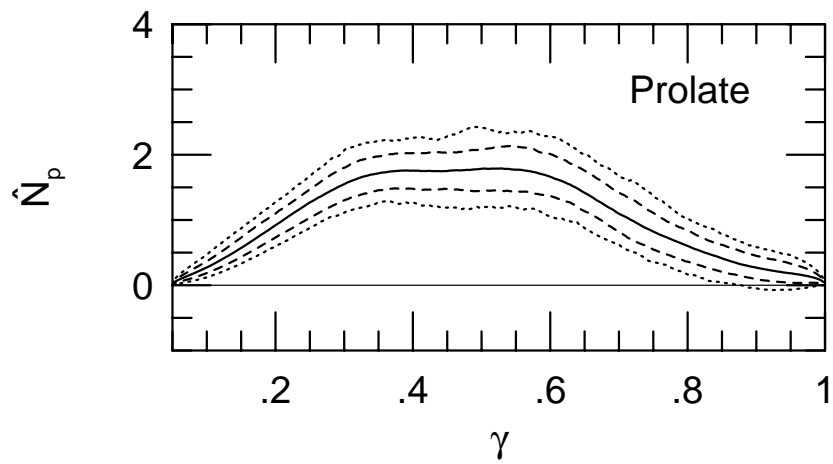
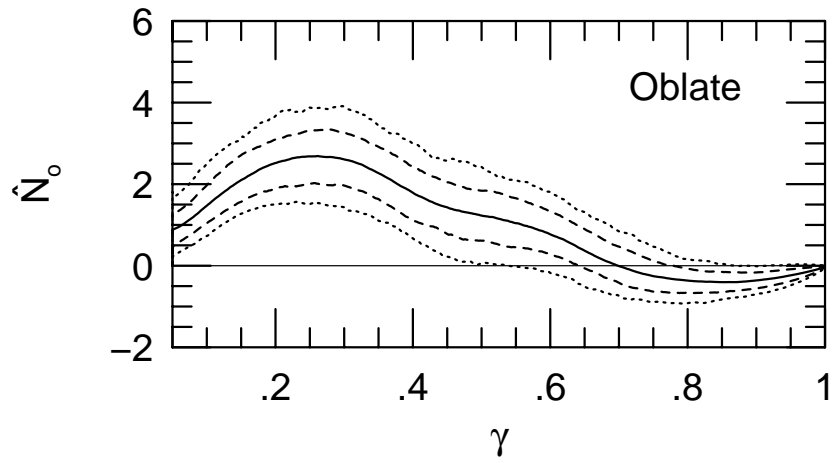
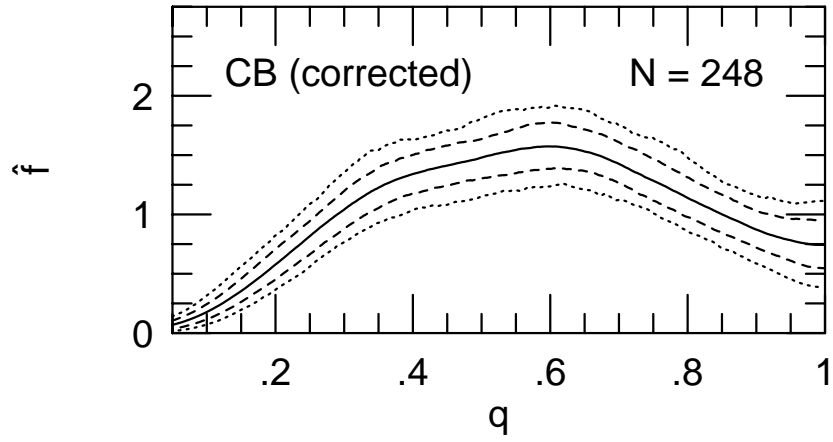
Fig. 5.— As Fig. 1, but for a sample of 19 dense cores, or “clumps”, in the Lynds 1630 (Orion B) molecular cloud (Lada, Bally, & Stark 1991). The kernel width is $h = 0.093$.

Fig. 6.— As Fig. 1, but for a sample of 89 dense cores in the ρ Ophiuchus molecular cloud complex (Loren 1989). The kernel width is $h = 0.074$.

Fig. 7.— As Fig. 1, but for a sample of 48 dense cores in the Ophiuchus dark cloud complex (Nozawa et al. 1991). The kernel width is $h = 0.090$.

Fig. 8.— As Fig. 1, but for a sample of 23 clouds in the Ophiuchus dark cloud complex (Nozawa et al. 1991). The kernel width is $h = 0.080$.





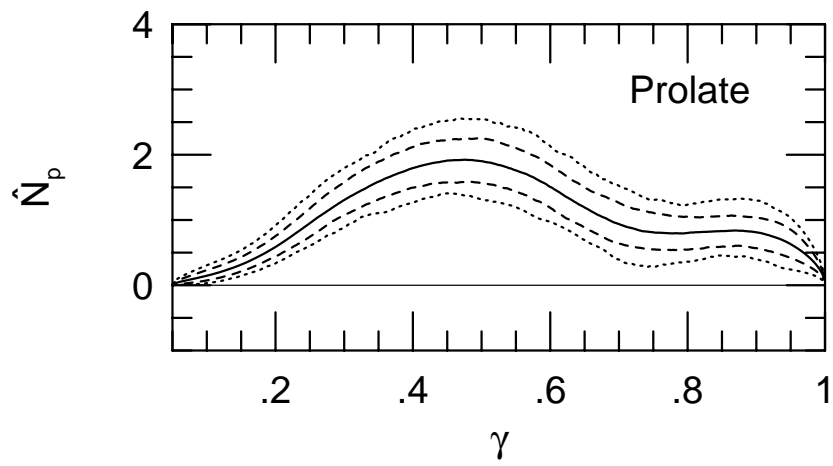
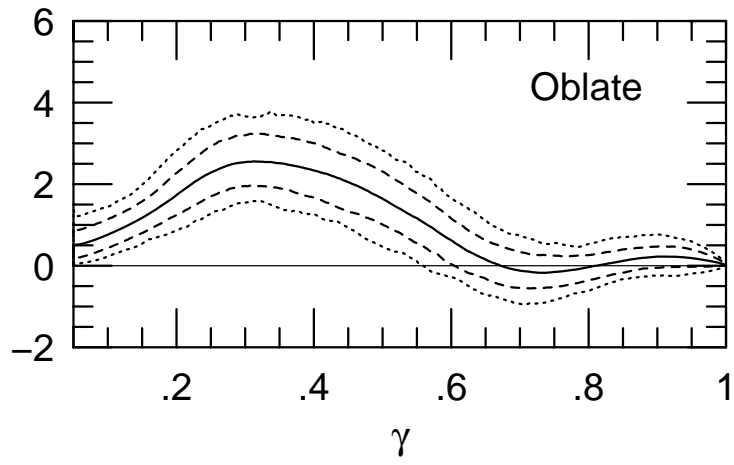
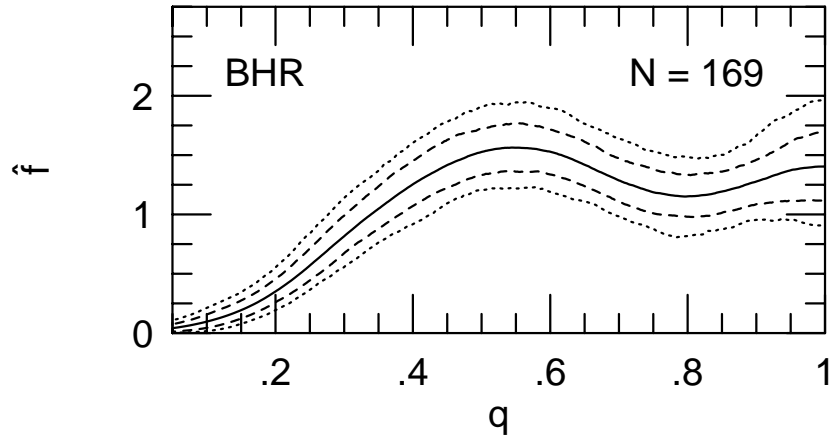


Fig. 4

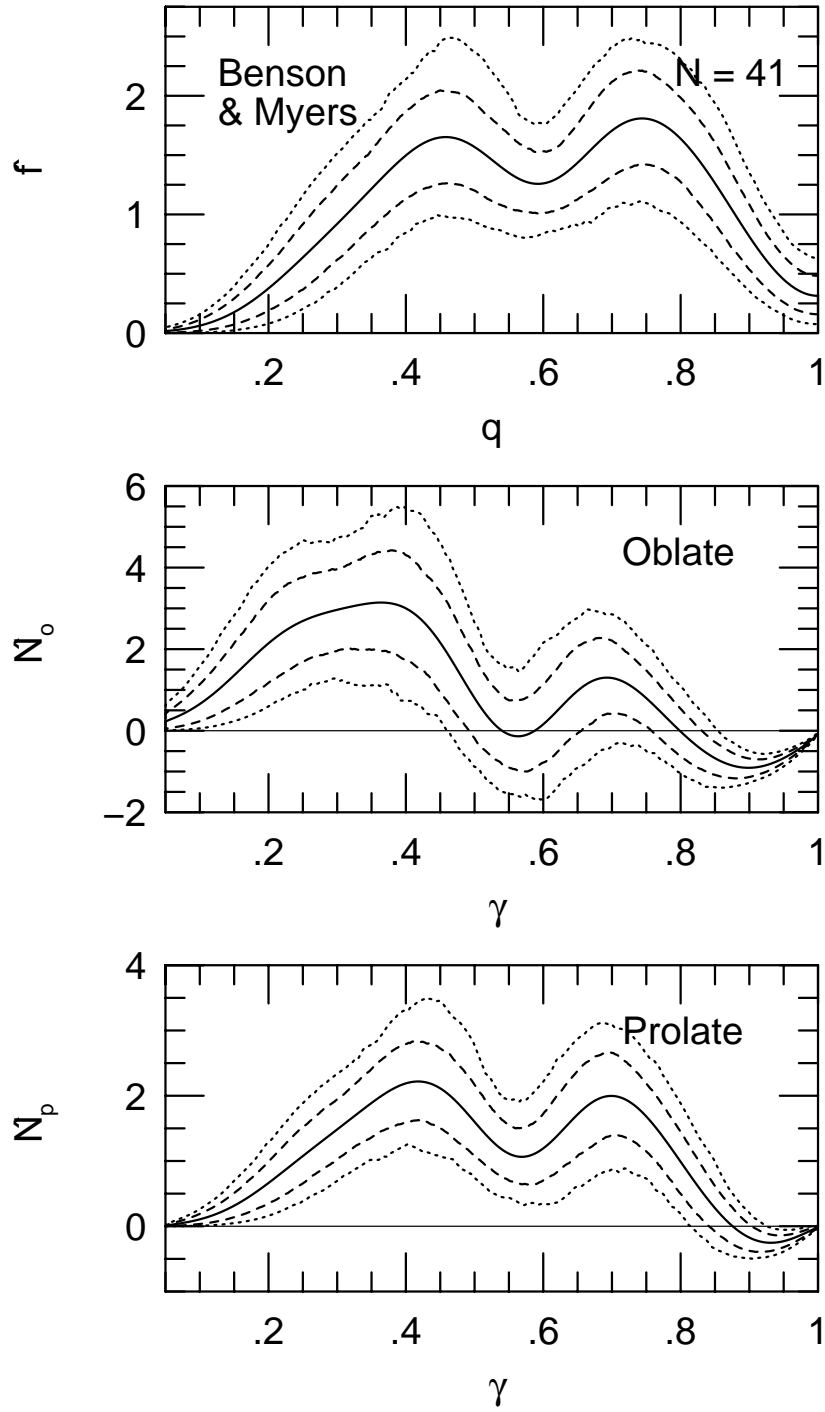
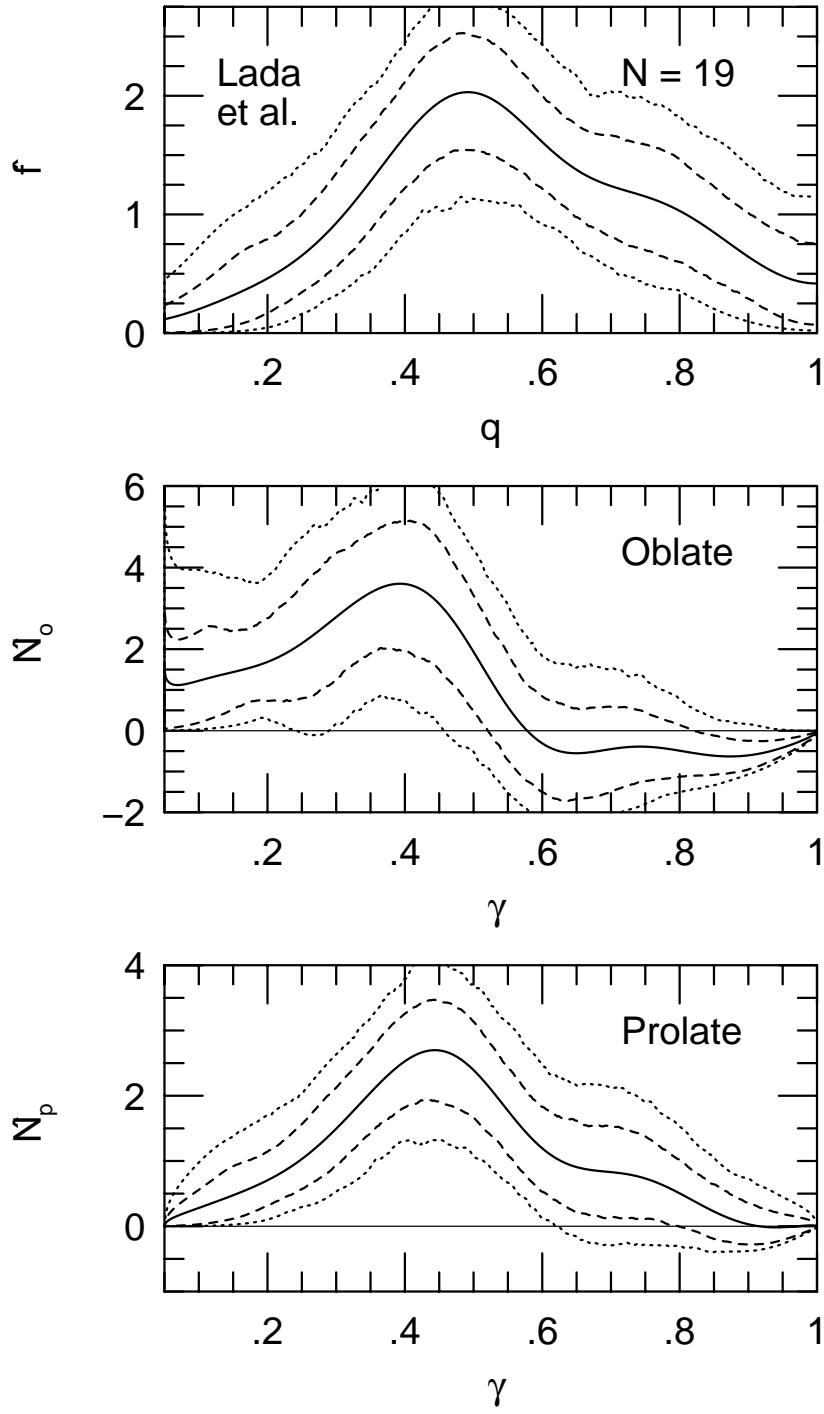


Fig. 5



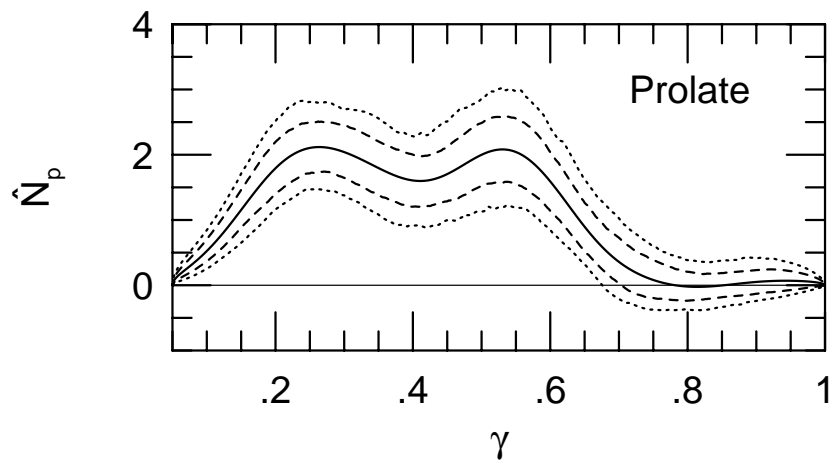
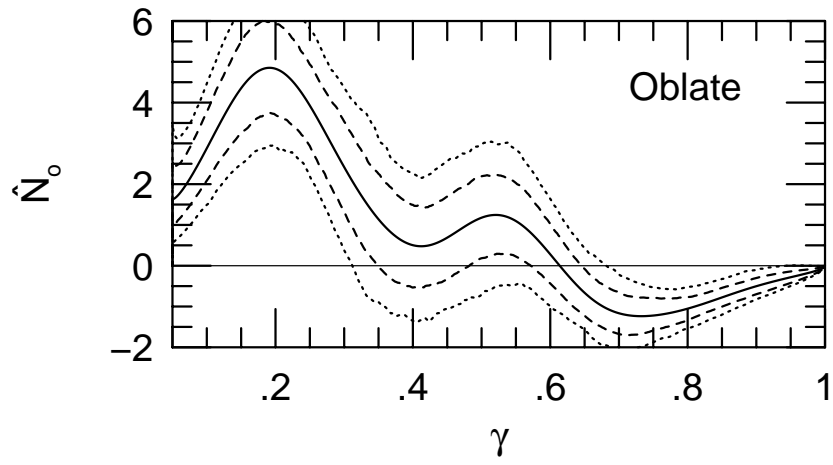
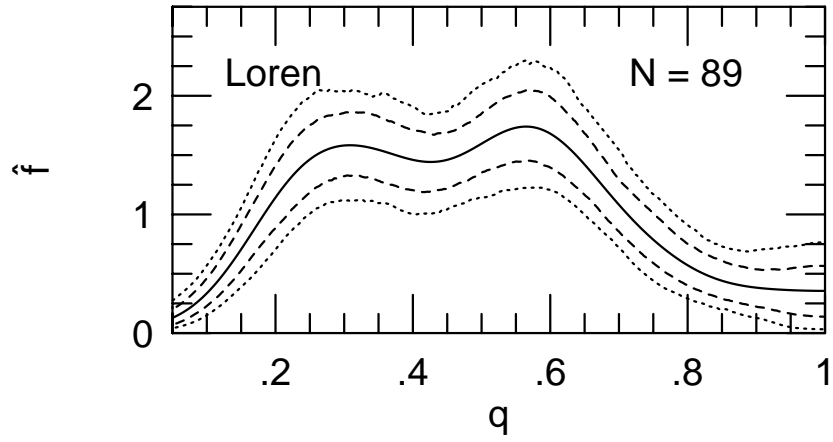


Fig. 7

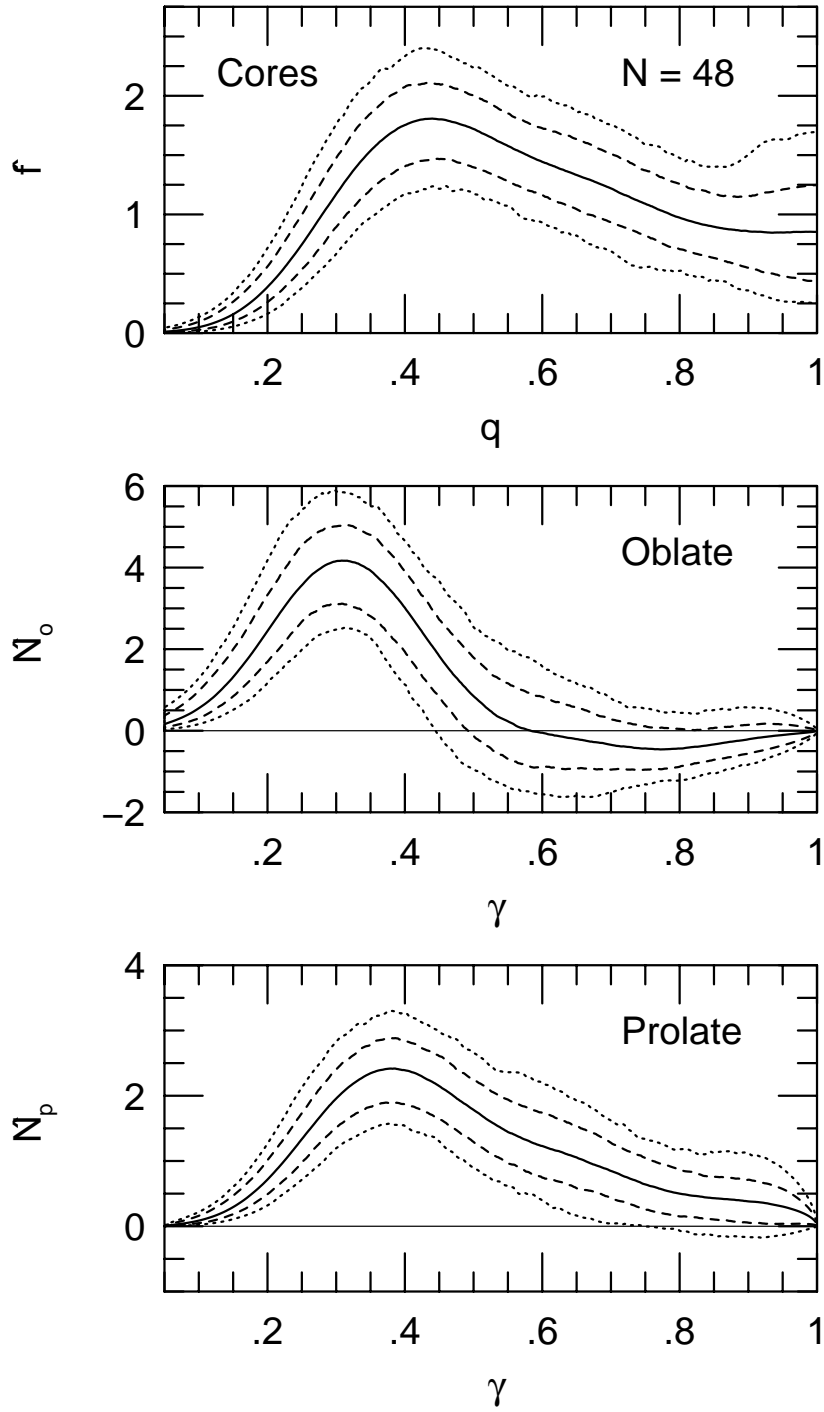


Fig. 8

